NANO LETTERS

2008
Vol. 8, No. 1
87−91

Intersubband Decay of 1-D Exciton Resonances in Carbon Nanotubes

Tobias Hertel,*,†,‡ Vasili Perebeinos,§ Jared Crochet,† Katharina Arnold,|| Manfred Kappes,|| and Phaedon Avouris§

Department of Physics and Astronomy, Vanderbilt University, Nashville, Tennessee 37235, Vanderbilt Institute for Nanoscale Science and Engineering, Vanderbilt University, Nashville, Tennessee 37235, IBM T. J. Watson Research Center, Yorktown Heights, New York 10598, and Institut für Nanotechnologie, Forschungszentrum Karlsruhe, and Institut für Physikalische Chemie, Universität Karlsruhe, Karlsruhe, Germany

Received August 20, 2007

ABSTRACT

We have studied intersubband decay of E_{22} excitons in semiconducting carbon nanotubes experimentally and theoretically. Photoluminescence excitation line widths of semiconducting nanotubes with chiral indicess (n,m) can be mapped onto a connectivity grid with curves of constant ($n - m$) and ($2n + m$). Moreover, the global behavior of E_{22} line widths is best characterized by a strong increase with energy irrespective of their (n-m)mod(3) = ±1 family affiliation. Solution of the Bethe–Salpeter equations shows that the E_{22} line widths are dominated by phonon assisted coupling to higher momentum states of the E_{11} and E_{12} exciton bands. The calculations also suggest that the branching ratio for decay into exciton bands vs free carrier bands, respectively is about 10:1.

The energetics and dynamics of excited states in carbon nanotubes (CNTs) receive attention because of their relevance for nonequilibrium carrier transport in nanotube electronic devices and their importance for a better understanding of photoluminescence quantum yields, branching ratios and other fundamental photophysical properties of CNTs.[1−6]

Photoluminescence spectroscopy of semiconducting carbon nanotubes has been extraordinarily useful not only in determining the energetics of excitons and their fine structure[7−9] but also for establishing detailed structure−property relationships.[10−13] Striking family patterns of tubes characterized by chiral indices (n,m) have been used to relate first and second subband exciton energies, E_{11} and E_{22}, respectively, and are found to lie on a grid of curves connecting tubes with constant ($n - m$) and constant ($2n + m$).[10] Moreover, tubes whose chiral indices are such that ($n - m$)mod(3) = −1 generally have large E_{22}/E_{11} ratios with values closer to 2 and those with ($n - m$)mod(3) = +1 have an E_{22}/E_{11} ratio significantly below 2.[10,14] Similar patterns, such as for strain and temperature dependence of exciton transitions, for example,[11−13] also indicate a strong sensitivity to chirality and tube structure. However, evidence for family relationships in the dynamical properties of excited states is scarce, and how strongly electronic or vibronic processes contribute to the exciton dynamics is not yet resolved.

Here, we examine family connectivities of exciton interband decay rates and their implications for exciton dynamics in semiconducting SWNTs. The observed family patterns in combination with solutions of the Bethe−Salpeter equation[15,16] allow us to identify zone boundary phonon scattering as the dominant facilitator for interband relaxation. Our calculations moreover show that the branching ratio for decay of the E_{22} exciton into the first subband e−h pair continuum and the lower lying exciton bands is about 1:10.

Single-wall carbon nanotube suspensions are prepared from commercial nanotube material (HiPCO, CNI Houston). We used two types of samples: type A made from soot ultrasonically dispersed and ultracentrifuged in D_2O using SDS as surfactant[17] which is here referred to as SDS-SWNT and type B made from nanotubes of the same raw material after isopycnic fractionation from H_2O nanotube suspensions with sodium cholate as surfactant[18,19] here referred to as SC-SWNT.

Photoluminescence excitation spectra from SDS-SWNTs were measured in the range 800−1700 nm with a Bruker Equinox 55S/FRA106 FT Raman spectrometer equipped with a liquid nitrogen cooled germanium detector[20] SC-SWNTs

* Corresponding author. E-mail: Tobias.hertel@vaderbilt.edu.
† Department of Physics and Astronomy, Vanderbilt University.
‡ Vanderbilt Institute for Nanoscale Science and Engineering, Vanderbilt University.
§ IBM T. J. Watson Research Center.
|| Universität Karlsruhe.

10.1021/nl0720915 CCC: $40.75
Published on Web 12/11/2007

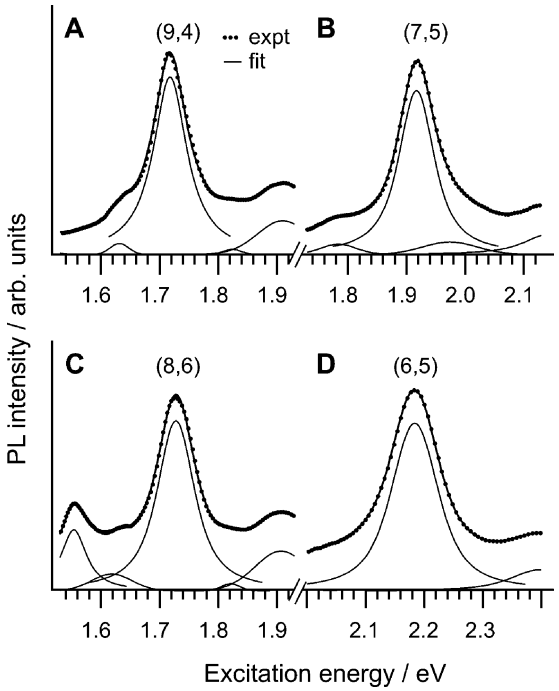

Figure 1. Four selected photoluminescence excitation spectra for emission from an (A) type sample at (a) 1109 nm, (b) 1031 nm, (c) 1180 nm, and (d) 983 nm. The center peaks in these spectra correspond to the E_{22} exciton resonances of (9,4), (7,5), (8,6), and (6,5) nanotubes, respectively. The thin solid line is the fit used to determine line widths.

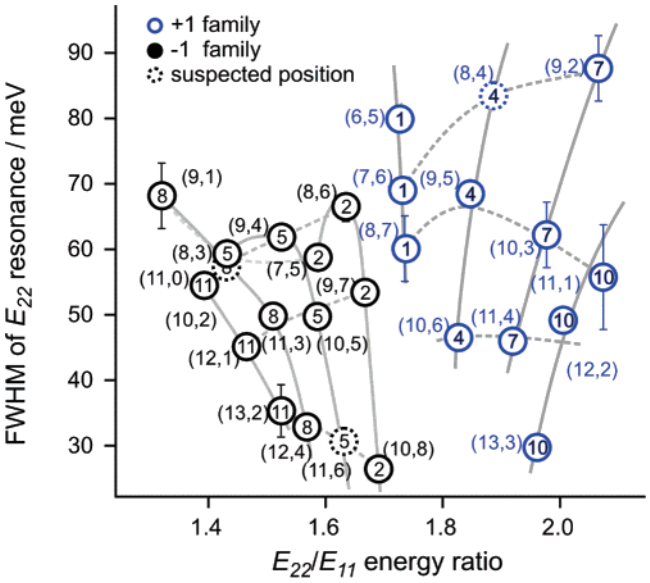

Figure 2. Photoluminescence excitation line widths versus the E_{22}/E_{11} ratio. The $(n - m)$ family affiliation is indicated by the corresponding numbers within the datapoints. Dashed lines connect tubes with the same $(2n + m)$.

were studied with a Jobin Yvon/Horiba Fluorolog-3 FL3-111 spectrophotofluorometer equipped with a liquid nitrogen cooled InGaAs detector. PL spectra were recorded with 8 nm excitation spectral slits and a 20 cm^{-1} resolution of the FT-Raman spectrometer and with 10 nm exitation slit width in the case of measurements performed with the Flurolog. Both sample types are found to have very similar excitation line widths. Small systematic deviations are mostly attributed to the different resolution of spectrometers used for both experiments.

A set of selected photoluminescence excitation spectra is reproduced in Figure 1 where we plot PL intensities at 1109, 1031, 1180, and 983 nm as a function of excitation wavelength. The center peaks in these spectra correspond to the E_{22} exciton resonances of (9,4), (7,5), (8,6), and (6,5) nanotubes, respectively. To extract the width of E_{22} exciton resonances we used a multi-Voigt peak, nonlinear least-squares fit routine with polynomial background subtraction. The routine is part of the IGOR software package (Wavemetrics) and uses the Levenberg−Marquardt algorithm for minimization of χ^2. The results of such a fit to select datasets are likewise shown in Figure 1 as solid lines. The estimated error margins are significantly larger than the confidence bands of the nonlinear least-squares fit and are based on the reproducibility of the fit if results from different datasets are compared including mismatch of the results obtained for SDS- and SC-SWNT samples. For the following discussion we corrected data for instrumental resolution. The line widths used later on thus include inhomogeneous broadening that is estimated to be on the order of 10 meV based on a comparison of line widths for E_{11} emission features from vacuum and surfactant suspended SWNTs (see for example ref 21).

To identify the mechanisms leading to the observed line widths, we begin with an investigation of their chirality and energy dependence. If we plot E_{22} line widths versus their respective $h\nu_{22}/h\nu_{11}$ energy ratios, for example, the data follow a striking family pattern where individual data points can be connected by a grid of intersecting curves with constant $(n - m)$ and $(2n + m)$ (see Figure 2). The numbers inside the datapoints give the $(n - m)$ family affiliation. Family connectivities with patterns similar to this one have previously been found for the photoluminescence excitation maps of semiconducting SWNTs[10] but also for the temperature and strain dependence of exciton line positions.[11−13] The lines with constant $(n - m)$ converge toward 1.7, the large-tube limit of the energy ratio $h\nu_{22}/h\nu_{11}$. The overall trend is for smaller tubes to have larger line widths, a trend which is reversed only by the smallest tubes of the −1 family studied here, specifically the (8,3) and (7,5) tubes.

To identify the microscopic process responsible for the observed family connectivity and for the width of E_{22} exciton resonances, we now search for correlations of line widths with established structural and electronic properties such as chirality, tube diameter, E_{11} or E_{22} transition energies, the $(h\nu_{22} - h\nu_{11})$ or $(h\nu_{22} - \Delta_{11}^{\Gamma})$ energy differences, where Δ_{11}^{Γ} refers to the free e−h pair generation threshold. Aside from the family connectivity discussed above, we find that the by far clearest and strongest correlation of E_{22} resonance widths is with the energy of the E_{22} resonance itself (see Figure 3). We also note that we find no evidence for an explicit dependence of line widths on the ±1 family affiliation, and the larger line widths of the +1 family tubes in Figure 2 can be exclusively attributed to a correlation with their higher E_{22} energies. This also implies that there is no

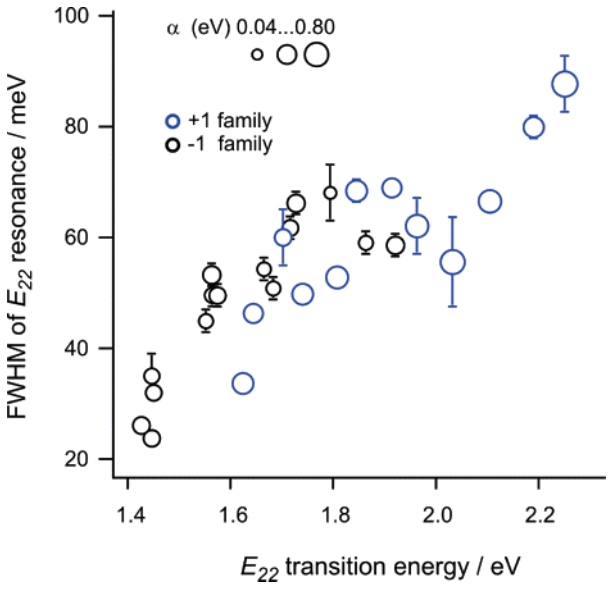

Figure 3. Global behavior of E_{22} line widths is best characterized by a pronounced energy dependence with no discernible influence of +1 or −1 family affiliation.

clear evidence that increase of the E_{22} energy above the $2h\nu_{11}$ threshold opens up an additional decay channel as suggested recently.[22]

To explore the pronounced energy dependence of resonance line widths in further detail, we consider the two microscopic mechanisms that can lead to energy relaxation from the E_{22} state. One is referred to as a phonon mechanism because it describes phonon mediated coupling of E_{22}^{Γ}, the Γ-point exciton to lower lying exciton states of the E_{11} and E_{12} manifolds at energies ($h\nu_{22} - \hbar\omega_q$) with momentum q (see left panel of Figure 4A). The second possible mechanism describes direct coupling of the E_{22} state to the Γ-point continuum of free e−h pair excitations with its threshold at Δ_{11}^{Γ}. If the rate of decay W_{el} for the electronic process is approximated using Fermi's Golden Rule, we obtain

$$W_{el} \propto |\langle\psi_{22}|V_{el}|\psi_{e-h}\rangle|^2 \rho_{e-h}(h\nu_{22})$$

where ψ_{22} and ψ_{e-h} are wavefunctions of the second subband exciton and the continuum state in the first subband into which the E_{22} exciton decays. V_{el} is the coupling term, and ρ_{e-h} is the joint density of states of the final state continuum. Accordingly, one would expect the dependence of W_{el} on the JDOS at the energy $h\nu_{22}$ to lead to a pronounced dependence of the fwhm on the band alignment of the E_{22} state with respect to the free carrier band edge. By a comparison of line widths with the alignment parameter $\alpha = h\nu_{22}^{\Gamma} - \Delta_{11}^{\Gamma}$ (see Figure 4a), we should therefore be able to assess the importance of the electronic process for E_{22} energy relaxation.

The alignment parameter α is determined using a combination of experimental data and theoretical considerations. Recent calculations suggest that exciton binding energies $E_{b,11}$ scale linearly with the renormalized free-carrier gap.[23] A similar scaling consequently also characterizes the relationship of E_{11} binding energies with the corresponding optical transition energies. By comparison of calculated[23] and experimental E_{11} binding and transition energies $E_{b,11}$ and $h\nu_{11}$, respectively,[7,8] we find $E_{b,11} = 0.31h\nu_{11}$ and the free carrier gap becomes $\Delta_{11}^{\Gamma} = 1.31h\nu_{11}$. We can thus determine the alignment parameter α(n,m). From this we find that the E_{22} state is in resonance with the free carrier continuum for all tubes studied here. Moreover, the absence of any correlation of line widths with α (see Figure 3) suggests that coupling to the free carrier continuum is weak. To put these findings on a more quantitative basis, we solved the Bethe−Salpeter equation, as described in ref 16, using a π-orbital tight-binding basis set with a hopping parameter $t_0 = 3.0$ eV. This allows us to determine line widths from the frequency dependence of the absorption coefficient ϵ_2.[16] In the electronic decay mechanism, the E_{22} exciton couples to the free e−h continuum, as schematically shown in the right panel of Figure 4A, leading to a Lorentzian absorption spectrum.[16,24] Several states of the Bethe−Salpeter equation

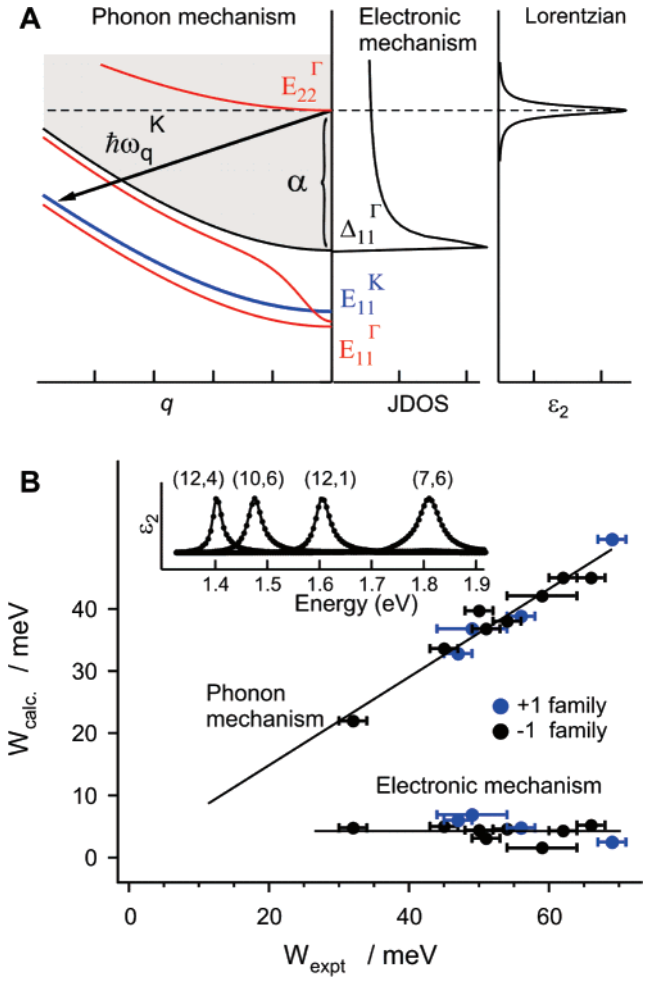

Figure 4. (A) Schematic illustration of two possible mechanisms leading to decay of the E_{22} exciton: (a) phonon mediated coupling to the E_{11} exciton bands (left side) and (b) decay by resonant coupling to the free e−h continuum (middle). (B) comparison of W_{expt} experimental E_{22} line widths with calculated ones (W_{calc}). Only the phonon mechanism shows a clear correlation between experiment and theory. The inset shows a selection of calculated excitation spectra with clearly increasing linwidths at higher excitation energies.

(BSE) contribute to the E_{22} exciton absorption. We choose a unit cell of about 500 nm length, large enough to resolve the spectral width of the E_{22} peak. The line widths resulting from the fit of Lorentz profiles to the calculated absorption spectra are shown in Figure 4B. However, the predicted broadening due to the electronic mechanism is, on average, a factor of 10 smaller than the experimental width and no correlation of calculated and experimental values is found.

The second decay mechanism discussed here involves exciton−phonon coupling, which allows the E_{22} exciton to decay to a lower energy state by phonon emission. Unlike in the electronic mechanism, which requires the initial exciton state and final electron−hole pair states to have the same angular and longitudinal momenta, namely $q = 0$, in the exciton−phonon mechanism, the phonon can have both finite angular and longitudinal momenta, resulting in a final state with finite momentum. To explore this phonon assisted E_{22} decay mechanism, we used the Su−Schrieffer−Heeger model[25,26] for the electron−phonon interaction, with a matrix element $t = t_0 - g\delta R_{C-C}$ dependent on the change of the nearest neighbor C−C distance δR_{C-C}. We use $g = 5.3$ eV/Å. Following ref 15, we calculate the exciton−phonon coupling using exciton wavefunctions from the BSE solution. We then use the Golden Rule to calculate the lifetime of each BSE state, which contributes to the E_{22} absorption spectra including the exciton−phonon coupling.[15] The E_{22} spectrum is then again fit with a Lorentzian profile with the resulting E_{22} fwhm plotted in Figure 4B to illustrate the clear correlation of theory and experiment. In our calculations, we allowed for E_{22} exciton coupling with all phonons and found that the E_{22} exciton primarily decays into the doubly degenerate dark E_{11} exciton[27] with a finite angular momentum via the zone-boundary K-optical phonon. The slope of the straight line fit to the calculated line widths using the phonon mechanism in Figure 4B is about 30% smaller than experimental data. Some of this difference may be due to phonon-assisted decay into σ states[28] as well as to thermal broadening by acoustic phonons on the order of a few millielectronvolts, which are not included in our theory.

The absence of any clear correlation of line widths and the family affiliation in the experiment is also consistent with the phonon decay mechanism. We note that there is a difference in the electron−phonon coupling for the two families in the single particle model.[29] However, the exciton binding energies also exhibit a family effect related to their effective masses.[16] As a result, the stronger bound excitons have larger exciton−phonon coupling,[15] which in effect compensates for the difference in the electron−phonon coupling in the single particle picture.[29] However, the complex family correlations seen experimentally in Figure 2 cannot be understood at this level of theory and may provide motivation to study these effects using more sophisticated approaches, for example, including the $\sigma-\pi$ orbital hybridization.

In conclusion, we find that line widths of the second subband E_{22} excitons in semiconducting carbon nanotubes exhibit pronounced family connectivities and strongly depend on the E_{22} transition energy. Our calculations show that the dominant scattering process to the lower lying dark E_{11} exciton subband is facilitated by coupling via zone boundary phonons from the E_{22} resonance. The line widths are found to be consistent with an e−ph coupling strength of about 5 eV/Å. In contrast, the coupling to the free carrier continuum is comparatively small and leads to a branching ratio for decay into the lower exciton versus free carrier bands of roughly 10:1. Future studies will need to clarify finer effects of the family connectivity of the relaxation rates.

Acknowledgment. J.C. and T.H. acknowledge support through a grant by the American Chemical Society (PRF 44479-AC10) and the National Science Foundation (DMR-0606505).

References

(1) Tans, S. J.; Verschueren, A. R. M.; Dekker, C. Room-temperature transistor based on a single carbon nanotube. *Nature* **1998**, *393* (6680), 49−52.
(2) Martel, R.; et al. Single- and multi-wall carbon nanotube field-effect transistors. *Appl. Phys. Lett.* **1998**, *73* (17), 2447−2449.
(3) Javey, A.; et al. Ballistic carbon nanotube field-effect transistors. *Nature* **2003**, *424* (6949), 654−657.
(4) Freitag, M.; et al. Electrically excited, localized infrared emission from single carbon nanotubes. *Nano Lett.* **2006**, *6* (7), 1425−1433.
(5) Misewich, J. A.; et al. Electrically induced optical emission from a carbon nanotube FET. *Science* **2003**, *300* (5620), 783−786.
(6) Marty, L.; et al. Exciton formation and annihilation during 1D impact excitation of carbon nanotubes. *Phys. Rev. Lett.* **2006**, *96* (13).
(7) Wang, F.; et al. The optical resonances in carbon nanotubes arise from excitons. *Science* **2005**, *308* (5723), 838−841.
(8) Maultzsch, J.; et al. Exciton binding energies in carbon nanotubes from two-photon photoluminescence. *Phys. Rev. B* **2005**, *72* (24).
(9) Mortimer, I. B.; Nicholas, R. J. Role of bright and dark excitons in the temperature-dependent photoluminescence of carbon nanotubes. *Phys. Rev. Lett.* **2007**, *98* (2).
(10) Bachilo, S. M.; et al. Structure-assigned optical spectra of single-walled carbon nanotubes. *Science* **2002**, *298* (5602), 2361−2366.
(11) Arnold, K.; et al. Matrix-imposed stress-induced shifts in the photoluminescence of single-walled carbon nanotubes at low temperatures. *Nano Lett.* **2004**, *4* (12), 2349−2354.
(12) Shan, W.; et al. Pressure dependence of optical transitions in semiconducting single-walled carbon nanotubes. *Phys. Status Solidi B-Basic Res.* **2004**, *241* (14), 3367−3373.
(13) Souza, A. G.; et al. Strain-induced interference effects on the resonance Raman cross section of carbon nanotubes. *Phys. Rev. Lett.* **2005**, *95* (21).
(14) Kane, C. L.; Mele, E. J. Ratio problem in single carbon nanotube fluorescence spectroscopy. *Phys. Rev. Lett.* **2003**, *90* (20).
(15) Perebeinos, V.; Tersoff, J.; Avouris, P. Effect of exciton-phonon coupling in the calculated optical absorption of carbon nanotubes. *Phys. Rev. Lett.* **2005**, *94* (2).
(16) Perebeinos, V.; Tersoff, J.; Avouris, P. Scaling of excitons in carbon nanotubes. *Phys. Rev. Lett.* **2004**, *92* (25).
(17) O'Connell, M. J.; et al. Band gap fluorescence from individual single-walled carbon nanotubes. *Science* **2002**, *297* (5581), 593−596.
(18) Arnold, M. S.; Stupp, S. I.; Hersam, M. C. Enrichment of single-walled carbon nanotubes by diameter in density gradients. *Nano Lett.* **2005**, *5* (4), 713−718.
(19) Crochet, J.; Clemens, M.; Hertel, T. Quantum Yield Heterogeneities of Aqueous Single-Wall Carbon Nanotube Suspensions. *J. Am. Chem. Soc.* **2007**, *129*, 8058−8059.
(20) Lebedkin, S.; et al. *FTIR-luminescence mapping of dispersed single-walled carbon nanotubes*. *New Journal of Physics* **2003**, *5*.
(21) Inoue, T.; et al. Diameter dependence of exciton-phonon interaction in individual single-walled carbon nanotubes studied by microphotoluminescence spectroscopy. *Phys. Rev. B* **2006**, *73* (23).
(22) Reich, S.; Thomsen, C.; Robertson, J. Exciton resonances quench the photoluminescence of zigzag carbon nanotubes. *Phys. Rev. Lett.* **2005**, *95* (7).
(23) Capaz, R. B.; et al. Diameter and chirality dependence of exciton properties in carbon nanotubes. *Phys. Rev. B* **2006**, *74* (12).

(24) Spataru, C. D.; et al. Excitonic effects and optical spectra of single-walled carbon nanotubes. *Phys. Rev. Lett.* **2004**, *92* (7).
(25) Su, W. P.; Schrieffer, J. R.; Heeger, A. J. Solitons in Polyacetylene. *Phys. Rev. Lett.* **1979**, *42* (25), 1698−1701.
(26) Su, W. P.; Schrieffer, J. R.; Heeger, A. J. Soliton Excitations in Polyacetylene. *Phys. Rev. B* **1980**, *22* (4), 2099−2111.
(27) Perebeinos, V.; Tersoff, J.; Avouris, P. Radiative lifetime of excitons in carbon nanotubes. *Nano Lett.* **2005**, *5* (12), 2495−2499.
(28) Blase, X.; et al. Hybridization Effects and Metallicity in Small Radius Carbon Nanotubes. *Phys. Rev. Lett.* **1994**, *72* (12), 1878−1881.
(29) Jiang, J.; et al. Exciton-photon, exciton-phonon matrix elements, and resonant Raman intensity of single-wall carbon nanotubes. *Phys. Rev. B* **2007**, *75*(3).

NL0720915